Animal Nutrition 20 (2025) 95–109

Contents lists available at ScienceDirect

Animal Nutrition

journal homepage: http://www.keaipublishing.com/en/journals/aninu/

Original Research Article

Metasilicate-based alkaline mineral water improves the growth performance of weaned piglets by maintaining gut-liver axis homeostasis through microbiota-mediated secondary bile acid pathway

Jian Chen [a, †], Kanwar K. Malhi [a, †], Xiaowei Li [a], Xiangwen Xu [a], Jianxun Kang [a], Bichen Zhao [a], Yaru Xu [a], Xuenan Li [a, b, c, *], Jinlong Li [a, b, c, *]

[a] College of Veterinary Medicine, Northeast Agricultural University, Harbin 150030 China
[b] Key Laboratory of the Provincial Education Department of Heilongjiang for Common Animal Disease Prevention and Treatment, Northeast Agricultural University, Harbin 150030, China
[c] Heilongjiang Key Laboratory for Laboratory Animals and Comparative Medicine, Northeast Agricultural University, Harbin 150030, China

ARTICLE INFO

Article history:
Received 3 November 2023
Received in revised form
31 August 2024
Accepted 19 September 2024
Available online 2 November 2024

Keywords:
Weaned piglet
Metasilicate-based alkaline mineral water
Gut-liver axis
Secondary bile acids
Cholesterol metabolism

ABSTRACT

Weaning stress causes substantial economic loss in the swine industry. Moreover, weaning-induced intestinal barrier damage and dysfunction of the gut-liver axis are associated with reduced growth performance in piglets. Metasilicate-based alkaline mineral water (AMW) has shown potential therapeutic effects on gastrointestinal disorders; however, the mechanisms involved and their overall effects on the gut-liver axis have not been explored. Here, sodium metasilicate (SMS) was used to prepare metasilicate-based AMW (basal water + 500 mg/L SMS). A total of 240 newly weaned piglets were allocated to the Control and SMS groups (6 replicate pens per group and 20 piglets per pen) for a 15-day trial period. Histopathological evaluations were conducted using hematoxylin and eosin staining. To analyze the composition of the gut microbiota, 16S rRNA PacBio SMRT Gene Full-Length Sequencing was performed. Western blotting and immunofluorescence were employed to assess protein expression levels. Our results indicated that metasilicate-based AMW effectively alleviated weaning-induced colonic or liver morphological injury and inflammatory response, as well as liver cholesterol metabolism disorders. Further analysis showed that metasilicate-based AMW promoted deoxycholic acid (DCA) biosynthesis by increasing the abundance of *Lactobacillus_delbrueckii* in the colon ($P < 0.001$). This consequently improved weaning-induced colon and liver injury and dysfunction through the DCA-secondary bile acid (SBA) receptors (SBAR)-nuclear factor-kappaB (NF-κB)/NOD-like receptor family pyrin domain-containing 3 (NLRP3) pathways. Growth performance parameters, including final body weight ($P = 0.034$) and average daily gain ($P < 0.001$), in the SMS group were significantly higher than those in the Control group. Therefore, metasilicate-based AMW maintains gut-liver axis homeostasis by regulating the microbiota-mediated SBA-SBAR pathway in piglets under weaning stress. Our research provides a new strategy for mitigating stress-induced gut-liver axis dysfunction in weaned piglets.

1. Introduction

When piglets are weaned from the sow, they encounter significant physiological, environmental, and social challenges, increasing their susceptibility to secondary diseases and production losses. Stress is considered an acute disturbance of body homeostasis, with both short- and long-term impacts on organ and system function (Campbell et al., 2013; Galluzzi et al., 2018). It is

* Corresponding authors.
E-mail addresses: Lixuenan@neau.edu.cn (X. Li), Jinlongli@neau.edu.cn (J. Li).
† These authors contributed equally to this paper.
Peer review under the responsibility of Chinese Association of Animal Science and Veterinary Medicine.

Production and Hosting by Elsevier on behalf of KeAi

https://doi.org/10.1016/j.aninu.2024.09.003

known that maintaining gut-liver axis homeostasis is essential for both animal and human health. The bidirectional interactions along the gut-liver axis can regulate gastrointestinal health and disease by utilizing environmental and host mediators (Pabst et al., 2023). Nutrients, metabolites, microbial antigens, and bile acids (BA) control immune responses and metabolism in the gut and liver, shaping microbial community structure and function reciprocally (Tilg et al., 2022). The disruption of host-microbiota crosstalk is implicated in the development of various liver diseases. This is primarily due to a damaged intestinal barrier which exacerbates hepatic inflammation and disease progression (Tilg et al., 2022). Evidence indicates that weaning stress can impair gut-hepatic system function leading to gut inflammation, barrier injury, malabsorption (Campbell et al., 2013; O'Mahony et al., 2009) as well as hepatic inflammation and disorders in glucolipid and cholesterol metabolism in piglets (Demori and Grasselli, 2023; Xu et al., 2022). Furthermore, stress-induced gut barrier injury and gut-liver axis disruption are linked to multiple liver diseases (Demori and Grasselli, 2023; Tilg et al., 2022). For instance, multiple lines of evidence from cellular, animal, and clinical studies suggest that stress-induced high cortisol levels and psychosocial stressors may contribute to the onset and worsening of metabolic (dysfunction)-associated fatty liver disease (MAFLD) (Eslam et al., 2020; Woods et al., 2015). Meanwhile, stress-induced dysfunction of the gut-liver axis is associated with diarrhea, immunity issues, and reduced growth performance in weaned piglets. Therefore, it is essential to develop an appropriate mitigation strategy for the weaned piglets that are at risk of stress exposure. Importantly, maintaining gut-liver axis homeostasis may be a promising target for alleviating subhealth states in weaned piglets.

Silicon, in addition to oxygen, is the second most abundant element in the Earth's crust and is one of the essential ingredients of life. While silicon is plentiful in many plant-based foods such as grains and barley, its bioavailability has been controversial due to the poor solubility (Bellia et al., 1994; Jugdaohsingh et al., 2008). Ortho-silicic acid and water-soluble silicates such as the widely accepted pharmaceutical sodium metasilicate (SMS) are bioavailable forms of silicon (Jurkic et al., 2013). Given its abundance in both humans and nature, silicon is expected to play a significant role in the body's health. However, despite its importance as a micronutrient, silicon has not received sufficient attention. Silicon is associated with various health benefits, including roles in Alzheimer's disease prevention, cardiovascular protection, immune system enhancement, collagen and bone tissue production, and other physiological processes (Jurkic et al., 2013). There is increasing evidence, both direct and indirect, supporting the antioxidant, anti-inflammatory, and damage repair effects of silicon. For instance, SMS has been shown to inhibit the release of nitric oxide (NO), tumor necrosis factor (TNF)-α, interleukin (IL)-6, and the expression of inducible nitric oxide synthase (*iNOS*) in mouse macrophages (Kim et al., 2013). Additionally, SMS can alleviate endothelial cell death under oxidative stress by stimulating angiogenic markers and antioxidant enzymes (Monte et al., 2018). However, most research has focused on the effects of SMS on skeletal growth and angiogenesis, leaving its impact on gut-liver axis homeostasis largely unexplored.

Water is an indispensable nutrient and plays a significant role in physiological and biochemical processes of the bidirectional interaction of the gut-liver axis (Carpino et al., 2022; Chen et al., 2023a,b). It is well known that the silicon content is also one of the criteria for judging high-quality natural mineral water. Of note, the biologically beneficial effects of metasilicate-based alkaline mineral water (AMW) have been demonstrated in piglets, including reducing diarrhea incidence, improving the gut barrier, and acting as a regulator of gut microflora to elevate the abundance of beneficial communities (Chen et al., 2023a; Gunathilaka et al., 2022). Emerging evidence indicates that the gut microflora is a key component in maintaining the homeostasis of the gut-liver axis under stress exposure (Demori and Grasselli, 2023). The microbiota or its metabolites are potential mediators of bidirectional interaction in this axis (Demori and Grasselli, 2023). Therefore, in this study, we explored the potential of metasilicate-based AMW to maintain gut-liver axis homeostasis in piglets under weaning stress through the microbiota or their metabolites, as well as the underlying mechanisms involved.

2. Materials and methods

2.1. Animal ethics statement

All procedures were performed following the National Institutes of Health Guide for the Care and Use of Laboratory Animals, and the experiments were approved by the Northeast Agricultural University (NEAU) Animal Ethics Committee (consent ID. NEAUEC202102415).

2.2. Animal and trial design

In this study, SMS was used to prepare metasilicate-based AMW (basal water + 500 mg/L SMS). An early-weaned piglet model was employed as previously described (Chen et al., 2023a; Gimsa et al., 2022). Briefly, a total of 240 piglets (Large White × Landrace × Duroc) with similar body weight (BW, 9.15 ± 0.22 kg) were selected from 40 sows in their second to fourth parity. Each litter consisted of six piglets (three males and three females) and were separated from the sows at 28 d of age. The piglets were then transferred to a completely unfamiliar environment, which included different feed sources, mixing with piglets from other litters, and different physical environments. To induce maximum weaning stress and social hierarchy stress, six piglets from the same litter were dispersed into six different replicates. Then, 12 replicates were randomly divided into two groups (6 replicate pens per group and 20 piglets per pen, $n = 120$): 1) Control group: provided basal water (pH = 7.0); and 2) SMS group: consumed metasilicate-based AMW (pH = 8.8). Consistent with our previous study (Chen et al., 2022), piglets received water ad libitum from two different tanks that were fitted with a water meter, agitator, and a reactor system: one tank contained basal water plus 500 mg/L SMS (metasilicate-based AMW, pH 8.8), and the second contained basal water without SMS supplementation (Control, pH 7.0).

All piglets received the same standard diet (NRC, 2012) (Table 1), and had ad libitum access to feed throughout the study (15 d). (2020), The levels of crude protein (GB/T 6432-2018), lysine (GB/T 18246-2000), threonine (GB/T 18246-2000), calcium (GB/T 6436-2018), and total phosphorus (GB/T 6437-2018) were measured according to the national standards of China . The initial BW, final BW and average daily feed intake (ADFI) of the experimental piglets were recorded. From these data, the average daily gain (ADG) and feed to gain (F:G) ratio were calculated. The dosage of SMS added to metasilicate-based AMW was determined based on the previous study (Chen et al., 2023a). All raw materials for SMS with food-grade purity were sourced from Nail Biotechnology Co., Ltd. (Beijing, China).

2.3. Sample harvest

The piglets were sacrificed following a procedure described previously (Chen et al., 2023b). Briefly, one piglet from each pen was chosen and euthanised with an intravenous injection of sodium pentobarbital (40 mg/kg) to collect samples ($n = 6$) and

Table 1
Composition and nutrient levels of the basal diet (as-fed basis, %).

Item	Content	Nutrient levels	Content
Corn	49.30	Calculated nutrient levels[2]	
Soybean meal	25.40	DE, Mcal/kg	3.35
Soy protein isolate	3.00	Methionine + cystine	0.81
Whey powder	7.50	Measured nutrient levels	
Soybean oil	1.50	Crude protein	21.51
Lactose	10.00	Lysine	1.41
Stone powder	0.75	Threonine	0.94
Calcium hydrogen phosphate	1.05	Calcium	0.86
50% choline chloride	0.10	Total phosphorus	0.70
Lysine	0.22		
L-Methionine	0.10		
L-Threonine	0.08		
Vitamin and mineral premix[1]	1.00		
Total	100.00		

[1] Vitamin and mineral premix supplied per kilogram diet: VA 18,000 IU; VD 4000 IU; VE 50 mg; VK_3 4 mg; VB_1 4 mg; VB_2 10 mg; VB_6 4 mg; VB_{12} 30 μg; pantothenic acid 30 mg; folic acid 2 mg; biotin 0.16 mg; Fe 150 mg; Cu 18 mg; Mn 48 mg; Zn 150 mg; I 1.5 mg; Se 0.3 mg.
[2] The digestible energy (DE) and methionine + cystine was calculated according to the Tables of Feed Composition and Nutritive Values in China (2020).

ensure humane and ethical treatment of the piglets. Blood samples (10 mL each) were collected from the jugular vein, and the serum was obtained by immediate centrifugation (3000 × *g* for 10 min, 4 °C) and kept at −80 °C for analysis. After opening the abdominal cavity, the mid-colon tissues of appropriate size were collected and placed in 4% paraformaldehyde or an ultra-low temperature refrigerator (−80 °C), respectively. The mid-colonic contents were harvested using sterile fecal tubes for 16S rRNA PacBio SMRT Gene Full-Length Sequencing.

2.4. Morphological observation

As previously described, hematoxylin and eosin (H&E) staining was used to examine the morphology of the colon (Li et al., 2024) and liver (Zhao et al., 2022). The DM2000 LED microscope (Leica, Germany) was used to observe the gut and liver sections. Consistent with the previous report, the total histological score of the colon was given as epithelium + infiltration (Ding and Wen, 2018). The scoring rules were as follows: 1) for epithelium, 0, no abnormal morphology; 1, goblet cells loss; 2, massive loss of goblet cells; 3, crypt loss; 4, massive loss of crypts; and 2) for infiltration, 0, no infiltrate; 1, infiltrate around the crypt basis; 2, infiltrate reaching the lamina muscularis mucosae; 3, extensive infiltration reaching the lamina muscularis mucosae and thickening of the mucosa with abundant edema; and 4, infiltration of the lamina submucosa. Additionally, to assess hepatic lipid accumulation, Oil Red O staining was performed, and the Oil Red O (+) area was quantified by Image J.

2.5. Enzyme-linked immunosorbent assay (ELISA) and secondary bile acid (SBA) determination

The collected serum, mid-colonic tissues or contents, and liver tissues were used to measure the levels of lipopolysaccharide (LPS), total bile acid (TBA), gut barrier marker (diamine oxidase[DAO]), blood biochemistry markers of liver function (alanine aminotransferase [ALT] and aspartate aminotransferase [AST]) and cholesterol (including total cholesterol [TC], and free cholesterol [FC]) by commercial kits following the manufacturer's protocol. Hepatic or serum cholesterol esters (CEs) levels were calculated by subtracting the TC content from the FC content. Standards and samples were added in triplicate; the absorbance was valued at 450 or 500 nm (Shi et al., 2024). The SBA determination of deoxycholic acid (DCA) and lithocholic acid (LCA) was performed as previously reported (Lei et al., 2022). The details of the commercial kits can be found in the supplementary materials (Table S1).

2.6. Quantitative real-time PCR (qRT-PCR)

Total RNA was extracted using RNAout reagent (TaKaRa, Dalian, China) and reverse transcribed using the TIANScript RT Kit (TIANGEN, Inc. Beijing, China). The primers used in this study for qRT-PCR (Table S2) were designed by Primer Premier software 6 (Zhang et al., 2024a). The reaction was performed on an ABI Quant Studio 5 Flex PCR instrument. The details of qRT-PCR profiles are consistent with our previous report (Dai et al., 2021). The relative mRNA level was calculated using the $2^{-\Delta\Delta Ct}$ method (Chen et al., 2024a).

2.7. Immunohistochemistry and immunoblotting

The details of the commercial antibodies used in this study can be found in the supplementary materials (Table S3). The preparation and processing of frozen sections and immunofluorescence staining are consistent with our previous study (Chen et al., 2023a). Briefly, samples were cut into 8 μm thick sections, washed with tris-buffered saline (TBS) solution, blocked with 10% goat serum for 0.5 h, incubated with the primary antibody working solution at 4 °C for 12 h, and then incubated with the corresponding secondary antibody at 37 °C for 1 h. The Leica fluorescence microscope (DMi8, Leica, Germany) was used for visualization after 4′,6-diamidino-2-phenylindole (DAPI) staining (10 min).

For Western blotting, the total proteins of tissues were separated by radio immunoprecipitation assay (RIPA) lysis buffer (Beyotime Biotechnology, Hangzhou, China). Protein samples were separated by 6%-10% sodium dodecyl sulfate-polyacrylamide gel electrophoresis (SDS-PAGE) and transferred onto a polyvinylidene fluoride (PVDF) or nitrocellulose (NC) membrane. The detailed procedure of Western blotting is shown in our previous report (Dai et al., 2022; Zhao et al., 2024). The PVDF or NC membranes containing proteins were washed five times, each for 6 min, and then imaged with the Amersham Imager 600 (GE, Switzerland). Image J software was employed to quantify blots or mean fluorescence intensity (National Institute of Health, USA).

2.8. Terminal deoxynucleotidyl transferase dUTP nick-end labeling (TUNEL) staining

TUNEL staining was performed according to the commercial kit instructions (Beyotime Biotechnology, Hangzhou, China). Briefly, the optimal cutting temperature (OCT) compound-embedded liver frozen sections were cut to an 8-μm thickness. The sections were washed twice with phosphate-buffered saline (PBS) solution for 10 min/time, incubated with 0.5% Triton X-100 for 5 min at room temperature and then incubated with the prepared TUNEL detection solution at 37 °C for 60 min. Cell nuclei were labeled with DAPI, and then fluorescent images were observed and collected with a fluorescence microscope (DMi8, Leica).

2.9. 16S rRNA sequencing of colonic microbiota

Total microbial genomic DNA from piglet colonic fecal samples was extracted following the manufacturer's instructions (TIANGEN Biotech Co., Ltd., Beijing, China, DP812) and stored in a refrigerator at −80 °C. The design of specific barcode sequencing primers, gene amplification, and sequencing library (SMRTbell library) formation

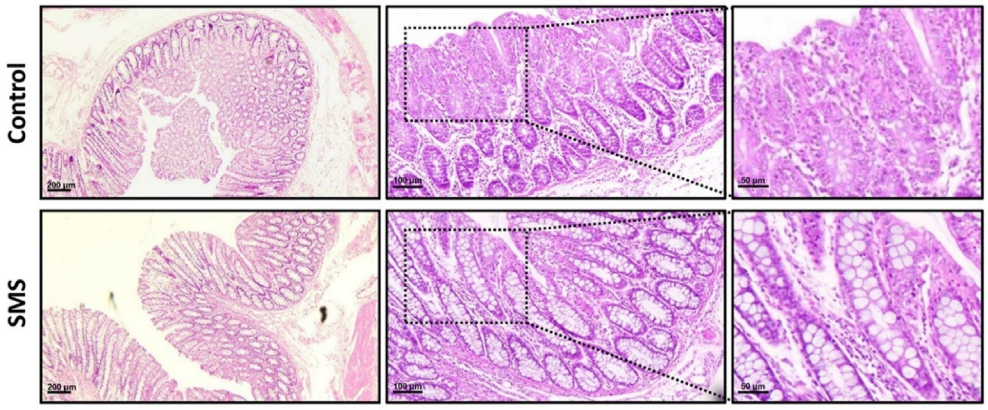

Fig. 1. Metasilicate-based alkaline mineral water alleviated colonic morphological injury in piglets under weaning stress. Representative imaging of colon hematoxylin and eosin staining. Control, piglets were provided with basal water; SMS, piglets consumed metasilicate-based alkaline mineral water (basal water + 500 mg/L sodium metasilicate).

was performed as described previously (Chen et al., 2023a). The formed library was checked, and the sequencing service was provided by Wekemo Tech Group Co., Ltd. (Shenzhen, China) using the PacBio Sequel System. A more detailed "bioinformatic analysis" of the colonic microbiota is provided in the supplementary information.

2.10. Statistical analysis

All data were analyzed using GraphPad Prism 9.0 (GraphPad Software, San Diego, CA, USA) software. All data were evaluated for normal distribution and homogeneous variance using the UNIVARIATE procedure. To compare the differences between the two groups, statistical analysis was performed using Student's *t*-test. The mathematical model for the *t*-test is:

$$Y_{ij} = \mu + T_i + \varepsilon_{ij},$$

where Y_{ij} refers to the observation of the dependent variable for the *j*-th sample in the *i*-th group; μ, the overall mean; T_i, the fixed effect of the *i*-th treatment (group); and ε_{ij}, the residual error for the observation. The difference in significance was set to 0.05 ($P < 0.05$), and all error deviations are described by ± standard deviation (SD). Comparison of alpha diversity (Chao1, Shannon, Simpson and observed_features indexes) between groups was performed using Welch's *t*-test and Wilcoxon rank test in the Quantitative Insights into Microbial Ecology Version (QIIME)2 software platform. β-diversity was analyzed using principal coordinate analysis (PCoA) and nonmetric multidimensional scaling (NMDS) based on the unweighted UniFrac distance in the QIIME (v1.80) software. Species comparison between groups was calculated by Welch's *t*-test and Wilcoxon rank test in the R project Vegan package (version 2.5.3). Redundancy analysis (RDA) and Pearson analysis were completed using the Wekemo bioincloud platform (https://http://www.bioincloud.tech/). Pearson's calculations were used to construct heatmap models for correlation analyses in R (Version 3.2.4). The specific descriptions of the statistical means are shown in the figure legends.

3. Results

3.1. Metasilicate-based AMW alleviates weaning stress-induced colonic injury in piglets

Given the susceptibility of the colon to stress and its critical role in the gut-liver axis, we evaluated the effect of metasilicate-based AMW on colonic epithelium injury in weaned piglets. As shown in Fig. 1, weaning stress caused obvious colonic crypt hyperplasia, extensive epithelial damage, and goblet cell loss. These lesions were significantly improved by metasilicate-based AMW treatment in piglets under weaning stress, as evidenced by the decreased colonic histology score (Table 2, $P < 0.001$). These results uncover that metasilicate-based AMW can attenuate the loss of gut epithelial integrity induced by weaning stress.

3.2. Metasilicate-based AMW ameliorates the gut microflora composition and function profiles in piglets under weaning stress

To investigate the role of the gut microflora in metasilicate-based AMW-mediated gut-liver axis homeostasis, colonic stool samples were collected for 16s rRNA sequencing. Rarefaction curves indicated that the depth of sequencing was sufficient to identify almost all bacterial species in the sample from this study (Fig. 2A). According to the results of the Chao1 ($P = 0.602$), Shannon ($P = 0.465$), and Simpson ($P = 0.251$) indexes, there was no difference in the α-diversity of colonic microbiota between the two groups (Figs. S1A–C). Surprisingly, SMS treatment induced significant alternations in colonic microbiota composition in weaned piglets, as manifested by PCoA (Fig. 2B) and Unweighted unifrac NMDS analysis (Fig. 2C). Then, to explore the specific changes in the microflora communities, a taxonomic analysis was performed at

Table 2
Effect of metasilicate-based alkaline mineral water on the colonic histology score and the levels of LPS and bile acids in colonic contents or serum of weaned piglets.[1]

Item	Control	SMS	SD	*P*-value
Colonic histology score	5.50	1.00	1.136	<0.001
Colonic contents, pg/g				
LPS	12.94	8.94	1.777	0.004
DCA	5.79	9.51	1.057	<0.001
LCA	2.43	3.76	1.045	0.052
Serum				
LPS, ng/L	328.10	270.10	26.925	0.004
DCA, pg/mL	8.72	17.16	1.854	<0.001
LCA, pg/mL	29.77	28.82	2.952	0.614
TBA, μmol/L	2.52	2.75	0.413	0.539

LPS = lipopolysaccharide; DCA = deoxycholic acid; LCA = lithocholic acid; TBA = total bile acid.
[1] Control, piglets were provided with basal water; SMS, piglets consumed metasilicate-based alkaline mineral water (basal water + 500 mg/L sodium metasilicate). Statistical significance was determined using Student's *t*-tests to compare differences between two groups; data are presented as the mean and standard deviation (SD); *P*-value less than 0.05 indicates a significant difference.

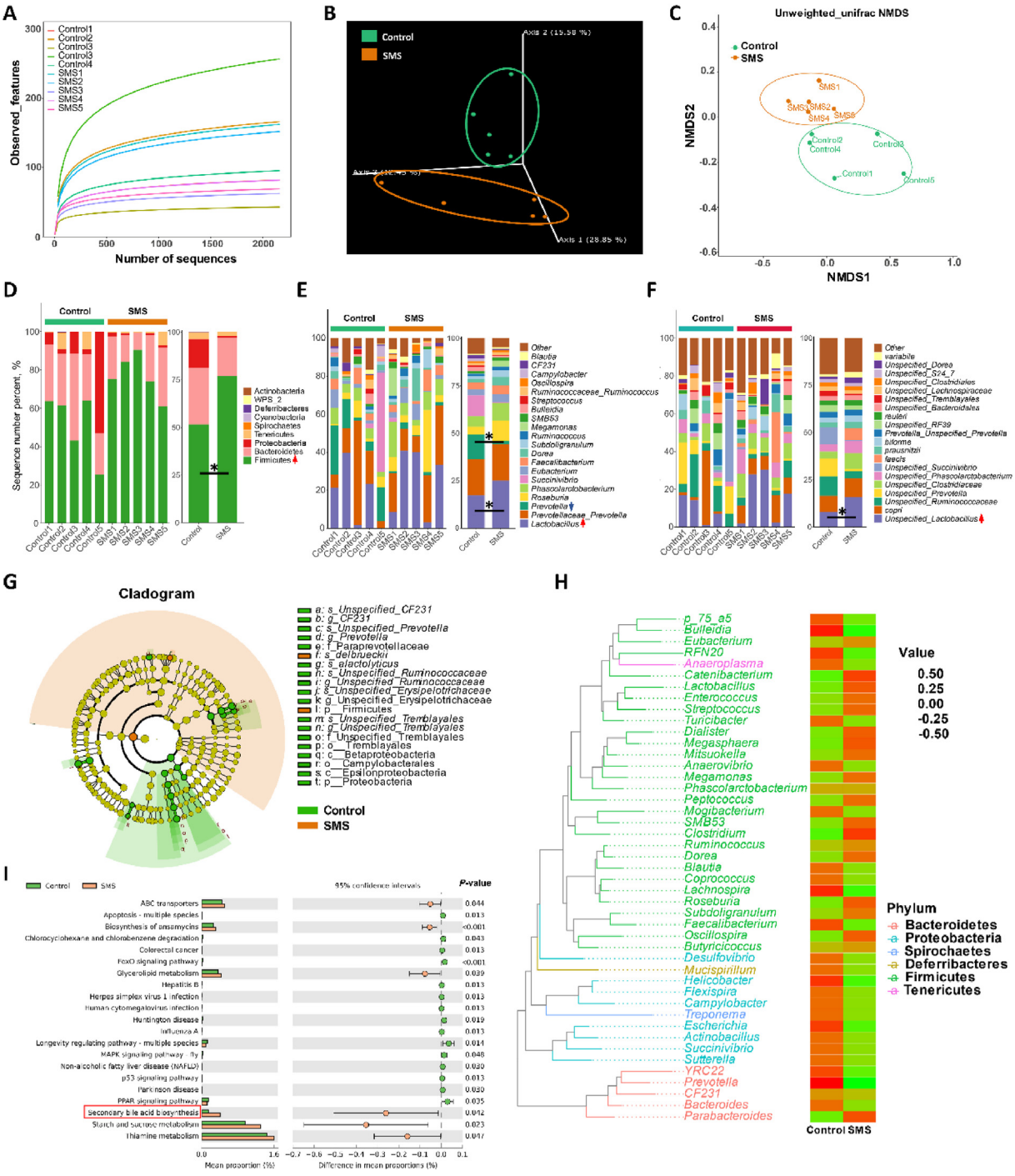

Fig. 2. Metasilicate-based alkaline mineral water ameliorated colonic microflora composition and function profiles in piglets exposed to weaning stress. (A) The rarefaction curve shown by each sample in bacterial communities. (B–C) The β-diversity of bacterial communities shown by (B) Principal coordinate analysis (PCoA) based on the unweighted UniFrac distance, and (C) Bray–Curtis Non-metric multidimensional scaling (NMDS). (D-F) Colonic microbial communities bar plot at the (D) phylum, (E) genus and (F) species level shown by each sample or groups. Blue arrow: decreased abundance; Red arrows: increased abundance. (G) Linear discriminant analysis effect size (LEFse) analysis on colonic biomarker microbiota. The size of the circles is based on relative abundance. The significantly different species using the nonparametric factorial Kruskal–Wallis rank sum test at a significance level of 0.05. (H) Phylogenetic tree and heatmap of abundance distribution between the Control group and SMS group. The "value" refers to the normalized relative abundance of the genus. (I) Difference histogram from Welch's *t*-test analysis for the relative abundances of bacterial Kyoto Encyclopedia of Genes and Genomes (KEGG) pathways between the Control group and SMS group. Control, piglets were provided with basal water; SMS, piglets consumed metasilicate-based alkaline mineral water (basal water + 500 mg/L sodium metasilicate). ABC = adenosine triphosphate (ATP)-binding cassette; FoxO = Forkhead box O; MAPK = mitogen-activated protein kinase; p53 = tumor protein p53; PPAR = peroxisome proliferator-activated receptors. Data are presented as the mean ± standard deviation (SD). *P*-value less than 0.05 indicates a significant difference. $^{*}P < 0.05$.

the levels of phylum (Fig. 2D), genus (Fig. 2E) and species (Fig. 2F). At the phylum level, although there were individual differences, the colonic microflora mainly included Firmicutes and Bacteroidetes in weaned piglets. Notably, Firmicutes abundance was significantly increased in colonic content after metasilicate-based AMW treatment. This shift contributed to an elevated Firmicutes/Bacteroidetes ratio (Fig. S1D, $P = 0.048$), which was considered a signal of gut microbiota homeostasis improvement. Moreover, after SMS

treatment, the changes in Firmicutes were supported by a significant increase in *Lactobacillus* abundance (a recognized beneficial microflora) at the genus and species levels (Fig. 2E–F, $P < 0.05$, red arrow). Conversely, the *Prevotella* genus, known for its LPS-metabolizing abilities, was enriched in the Control group's colonic feces compared to the SMS group (Fig. 2E, $P = 0.030$, blue arrow).

To identify marker bacteria between treatments, LEfSe analysis was employed on colonic microflora. As shown in Fig. 2G, the LEfSe analysis showed that in the Control group, biomarker bacteria included *unspecified_CF231* ($P = 0.037$), *unspecified_Prevotrlla* ($P = 0.037$), *Alactolyticus* ($P = 0.049$), *unspecified_Ruminococcaceae* ($P = 0.037$), *unspecified_Erysipelotrichaceae* ($P = 0.020$), and *unspecified_Tremblayales* ($P = 0.025$), whereas metasilicate-based AMW treatment shifted the marker community towards *Lactobacillus_delbrueckii* ($P = 0.048$) at the species level. Furthermore, phylogenetic tree and abundance distribution heatmap analyses highlighted significant alterations in dominant genera within each phylum, particularly increased the abundance of Firmicutes after SMS treatment (Fig. 2H). These results suggested that the interaction profiles of the colonic microbiota in both groups may change. As shown in Fig. S1E, we confirmed this speculation through microflora interaction analysis. Meanwhile, we found that the interaction nodes of *Lactobacillus* in the SMS group were more complex than those in the Control group, suggesting that at the genus level, *Lactobacillus* played a dominant role in piglets. Therefore, we speculated that the microflora community interaction network may be accompanied by a change in functional profiles. Comparing the sequencing data with the Kyoto Encyclopedia of Genes and Genomes (KEGG) pathway database by PICRUSt2 (Fig. 2I), the results showed that metasilicate-based AMW notably inhibited the abundance of genes involved in disease infection, such as colorectal cancer, Parkinson's disease, herpes simplex virus 1 infection, and influenza. Additionally, SMS treatment markedly reduced genes related to apoptosis and its regulatory signaling, including mitogen-activated protein kinase (MAPK), Forkhead box O (FoxO), and tumor protein p53 (p53) pathways. Likewise, it was worth emphasizing that the abundance of genes related to nonalcoholic fatty liver disease (NAFLD, similar to MAFLD) was decreased in colonic microbiota after SMS treatment, while genes involved in SBA synthesis were remarkably elevated, suggesting that improved gut microbiota composition may contribute to gut-liver axis homeostasis by modulating SBA synthesis.

3.3. Metasilicate-based AMW promotes DCA biosynthesis in piglets under weaning stress

Based on the results of colonic microbiota taxonomic and functional profile analysis, we speculated that bacterial metabolites LPS and SBA may mediate the regulation of the gut-liver axis in piglets under weaning stress. As expected, the content of the gram-negative bacterial metabolite LPS in colon feces was conspicuously reduced after SMS treatment (Table 2, $P = 0.004$). On the other hand, SBAs, primarily DCA and LCA, are among the most abundant microbiota metabolites and play a crucial role in gut-liver interactions. In this study, SMS treatment markedly increased DCA levels in both the colon and serum (Table 2, $P < 0.05$), suggesting an enhanced abundance of microflora involved in SBA synthesis. However, no significant differences were observed in LCA ($P = 0.052$ and $P = 0.614$) and TBA ($P = 0.539$) levels between the two groups (Table 2). Then, to identify the key communities responsible for LPS and DCA production, we conducted a series of analyses. RDA analysis revealed a positive correlation between LPS levels and *unclassified_Tremblayales* species and a negative correlation with the *Lactobacillus*. In addition, DCA biosynthesis was significantly positively correlated with *Lactobacillus delbrueckii* (Fig. 3A). Further analysis showed that the colonic marker microflora *L. delbrueckii* was notably correlated with decreased LPS ($P = 0.008$) and increased DCA ($P = 0.001$) after SMS treatment (Fig. 3B–C). These results suggest that microflora-derived LPS and DCA are key mediators of gut-liver axis homeostasis in piglets under weaning stress.

3.4. Microflora-mediated DCA alleviates colonic inflammation by activating the Takeda G protein-coupled receptor 5 (TGR5)/constitutive androstane receptor (CAR)/pregnane X receptor (PXR)-nuclear factor-kappaB (NF-κB) pathways in piglets under weaning stress

SBA mediates the regulation of the gut-liver axis through multiple receptors, including TGR5, vitamin D receptor (VDR), Farnesoid X receptor (FXR), CAR, PXR, glucocorticoid receptor (GR), and integrin alpha-5 beta-1 (α5β1). The qRT-PCR results indicated that SMS-induced DCA significantly activated *TGR5* ($P < 0.001$), *CAR* ($P = 0.005$), and *PXR* ($P = 0.001$) in the colon of weaned piglets but did not affect the expression of other SBA receptors (Fig. 4A). Moreover, the protein expression (Fig. 4B) of TGR5 ($P = 0.036$), CAR ($P = 0.001$), and PXR ($P = 0.032$) and the immunofluorescence density of CAR (Fig. 4C, $P = 0.003$) also supported this result. Colonic inflammation is a primary internal cause of stress-induced gut-liver axis dysfunction. Our results revealed that SMS treatment notably suppressed colonic NF-κB pathway activity (Fig. 4D) and inflammatory cell infiltration (Fig. 4E–F), as evidenced by decreased protein levels of Toll-like receptor 4 (TLR4, $P = 0.038$), myeloid differentiation factor 88 (Myd88, $P = 0.006$), NF-κB p65 (p65, $P = 0.023$), phosphorylated-p65 (p-p65, $P = 0.002$), and increased NF-κB inhibitor alpha (IκB-α, $P = 0.001$). Moreover, the fluorescence intensity of F4/80 (a macrophage marker, $P = 0.003$) and p65 ($P = 0.027$) was also reduced by SMS treatment. Consistent with these results, SMS markedly decreased pro-inflammatory factors (Fig. 4G), including TNF-α ($P = 0.010$), IL-1β ($P = 0.005$) and IL-6 ($P = 0.010$), while promoting the expression of the anti-inflammatory factor transforming growth factor-β (TGF-β, $P = 0.008$). These results indicate that metasilicate-based AMW-induced microflora-derived DCA can alleviate colonic inflammation by activating the SBA receptor (TGR5/CAR/PXR) pathways.

3.5. Microflora-mediated DCA relieves liver inflammation through the TGR5-NF-κB/NOD-like receptor family pyrin domain containing 3 (NLRP3) pathways in piglets under weaning stress

In this study, metasilicate-based AMW prominently reduced colonic barrier permeability in weaned piglets, as evidenced by decreased serum levels of DAO (Table 3, $P = 0.007$) and LPS (Table 2, $P = 0.004$). Importantly, this reduction was also implicitly supported by lower levels of liver function biochemical markers ALT (Table 3, $P < 0.001$) and AST (Table 3, $P = 0.013$), and alleviated hepatic morphological injury in weaned piglets treated with metasilicate-based AMW (Fig. 5A). Subsequently, to investigate the role of microflora-mediated DCA synthesis in alleviating liver injury, we analyzed the activity of SBA receptor signaling and its mediated inflammatory pathway. As shown in Fig. 5B, SMS treatment only activated liver *TGR5* ($P = 0.023$), with no significant effect on other receptors ($P > 0.05$). Moreover, similar to the colon, the hepatic NF-κB signaling pathway was inhibited by SMS treatment (Fig. 5C, $P < 0.05$). SMS treatment also hindered the NLRP3 inflammasome pathway (Fig. 5D), as reflected by decreased protein levels of NLRP3 ($P = 0.005$), apoptosis-associated speck-like protein containing a CARD (ASC, $P = 0.026$) and caspase-1 (Cas-1, $P = 0.022$). Furthermore, the reduction in pro-inflammatory factors (TNF-α, $P = 0.026$; IL-1β, $P = 0.031$; and IL-6, $P = 0.010$; Fig. 5E) and

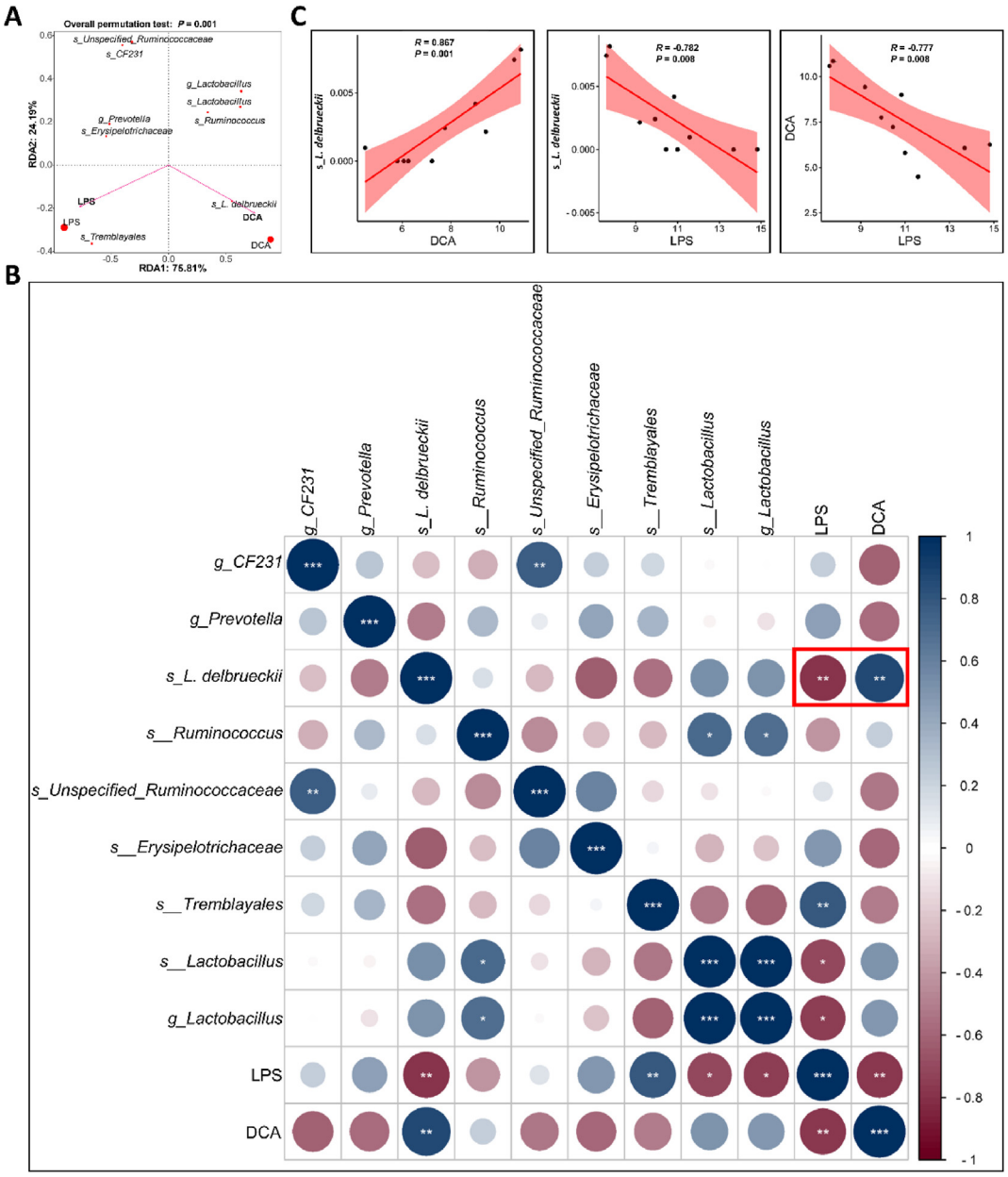

Fig. 3. Metasilicate-based alkaline mineral water promoted secondary bile acids biosynthesis by improving colonic microflora composition in piglets under weaning stress. (A) Redundancy analysis (RDA) for the relevance of colonic dominant microbiota with lipopolysaccharide (LPS) and deoxycholic acid (DCA) levels. (B) Correlation analysis between colonic dominant microbiota and LPS/DCA levels. Red box: correlation between the abundance of *s_L. delbrueckii* and levels of LPS and DCA. (C) Pearson correlation coefficient scatterplot among the *s_ L. delbrueckii* abundance, DCA and LPS levels. Data are presented as the mean ± standard deviation (SD). Statistical analysis was performed using Student's *t*-tests to compare differences between the two groups. *P*-value less than 0.05 indicates a significant difference. **P* < 0.05, ***P* < 0.01, and ****P* < 0.001.

the fluorescence intensity of p65 (Fig. 5F, $P = 0.048$), as well as the relief of macrophage infiltration (F4/80 density, $P = 0.024$) further confirmed that SMS-induced microflora-mediated DCA alleviated liver inflammation. Additionally, the attenuation of the inflammatory response further relieved hepatocyte apoptosis in weaned piglets (Fig. 5G, $P < 0.001$) after drinking metasilicate-based AMW. These results suggest that metasilicate-based AMW-induced DCA synthesis plays a vital role in alleviating liver inflammation through the TGR5-NF-κB/NLRP3 pathways.

3.6. Metasilicate-based AMW maintains liver cholesterol homeostasis by regulating the BA metabolism pathway

As shown in Fig. 6A, metasilicate-based AMW alleviated stress-induced liver lipid accumulation in weaned piglets, as reflected by the oil red O staining result ($P = 0.004$). As shown in Table 4, TC and FC levels (a lipotoxic molecule) in the serum ($P = 0.044$ and $P = 0.009$) and liver ($P = 0.017$ and $P = 0.012$) were markedly reduced after drinking metasilicate-based AMW. Meanwhile, CEs

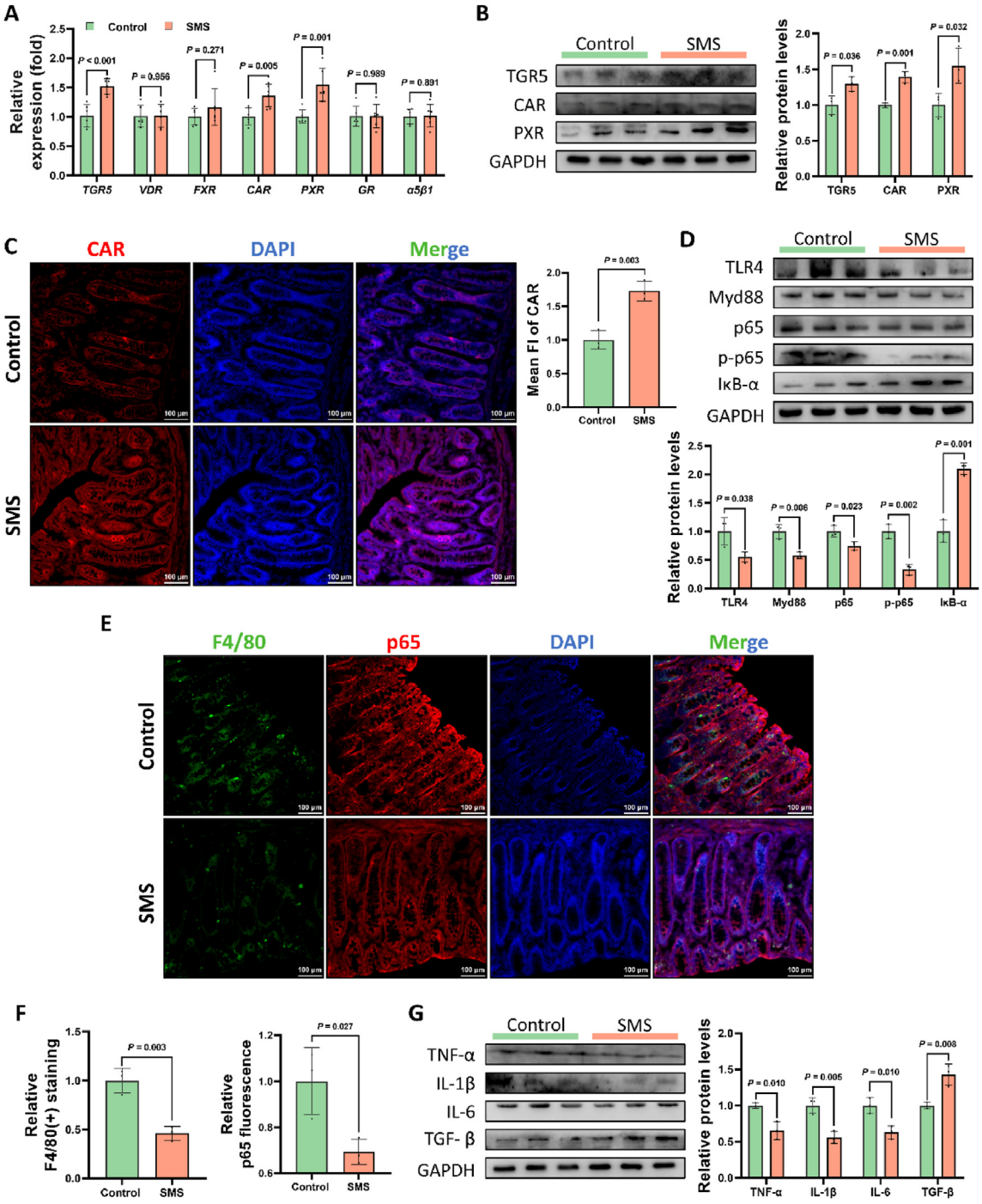

Fig. 4. Microflora-mediated secondary bile acids relieved colonic inflammation by activating secondary bile acids receptor pathway in piglets under weaning stress. (A) Statistical analysis of mRNA relative expression levels of secondary bile acids receptor *TGR5*, *VDR*, *FXR*, *CAR*, *PXR*, *GR*, and *α5β1* in the colon. (B) Statistical analysis of TGR5, CAR, and PXR protein levels. (C) Immunofluorescence images of CAR staining (red) and 4′,6-diamidino-2-phenylindole (DAPI, blue) of colon in weaned piglets and statistical analysis of CAR mean fluorescence intensity. (D) Statistical analysis of TLR4, Myd88, p65, p-p65, and IκB-α protein levels. (E) Immunofluorescence images of F4/80 staining (green), p65 staining (red) and DAPI (blue) in the colon. (F) Statistical analysis of F4/80-positive staining and p65 fluorescence intensity. (G) Statistical analysis of TNF-α, IL-1β, IL-6, and TGF-β protein levels. TGR5 = Takeda G protein-coupled receptor 5; VDR = vitamin D receptor; FXR = Farnesoid X receptor; CAR = constitutive androstane receptor; PXR = pregnane X receptor; GR = glucocorticoid receptor; α5β1 = integrin alpha-5 beta-1; TLR4 = Toll-like receptor 4; Myd88 = myeloid differentiation factor 88; p65 = nuclear factor-kappaB (NF-κB) p65; p-p65 = phosphorylated-p65; IκB-α = NF-κB inhibitor alpha; TNF-α = tumor necrosis factor-α; IL-1β = interleukin-1β; IL-6 = interleukin-6; TGF-β = transforming growth factor-β; GAPDH = glyceraldehyde 3-phosphate dehydrogenase; FI = fluorescent intensity. Control, piglets were provided with basal water; SMS, piglets consumed metasilicate-based alkaline mineral water (basal water + 500 mg/L sodium metasilicate). Data are presented as the mean ± standard deviation (SD). Statistical analysis was performed using Student's *t*-tests to compare differences between the two groups. *P*-value less than 0.05 indicates a significant difference.

Table 3
Effect of metasilicate-base alkaline mineral water on the DAO and liver function biochemical marker levels in the serum of weaned piglets.[1]

Item	Control	SMS	SD	*P*-value
DAO, pg/mL	107.90	78.37	13.628	0.007
ALT, U/L	17.74	13.41	1.320	<0.001
AST, U/L	19.88	14.07	3.319	0.013

DAO = diamine oxidase; ALT = alanine aminotransferase; AST = aspartate aminotransferase.
[1] Control, piglets were provided with basal water; SMS, piglets consumed metasilicate-based alkaline mineral water (basal water + 500 mg/L sodium metasilicate). Statistical significance was determined using Student's *t*-tests to compare differences between two groups; data are presented as the mean and standard deviation (SD). *P*-value less than 0.05 indicates a significant difference.

levels in the serum ($P = 0.045$) or liver ($P = 0.023$) were also significantly promoted, which is an important way for the liver to excrete FC. Additionally, the expression of liver acyl-coenzyme A: cholesterol acyltransferase 2 (ACAT2), a key enzyme for converting FC into CEs, was prominently enhanced after SMS treatment (Fig. 6B, $P = 0.013$), whereas the expression of StAR-related lipid transfer protein 4 (STARD4) showed no differences between the two groups ($P = 0.636$). Of note, metasilicate-based AMW did not affect factors related to cholesterol excretion (ATP-binding cassette transporter family A protein 1 [ABCA1], $P = 0.912$ and ATP-binding cassette subfamily G member 5 or G member 8 [*ABCG5/8*], $P = 0.736$ and $P = 0.262$), synthesis (3-hydroxy-3-methylglutaryl-CoA reductase [HMGCR], $P = 0.071$), or intake (low-density lipoprotein

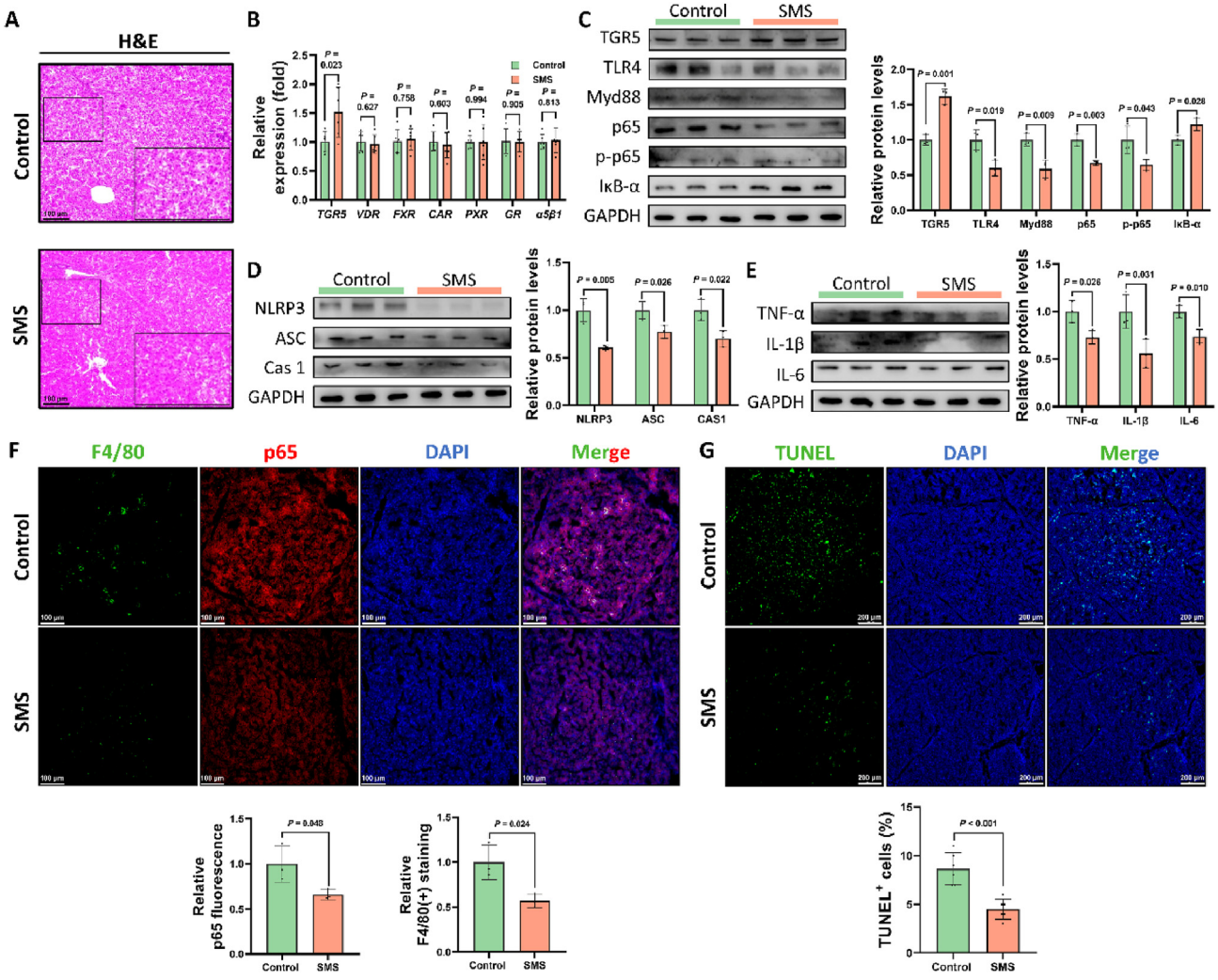

Fig. 5. Microflora-mediated DCA relieved liver dysfunction through the TGR5-NF-κB/NLRP3 pathways in piglets under weaning stress. (A) Hematoxylin and eosin (H&E) staining of liver tissue sections. (B) Statistical analysis of mRNA relative expression levels of secondary bile acids receptor *TGR5*, *VDR*, *FXR*, *CAR*, *PXR*, *GR*, and *α5β1* in the liver. (C) Statistical analysis of protein levels of secondary bile acid receptor TGR5 and NF-κB signaling pathway (TLR4, Myd88, p65, p-p65, and IκB-α) in the liver. (D) Statistical analysis of protein levels of NLRP3 inflammasome pathway (NLRP3, ASC, and Cas-1) in the liver. (E) Statistical analysis of proinflammatory factors TNF-α, IL-1β, IL-6 levels in the liver. (F) Immunofluorescence images of F4/80 staining (green), p65 staining (red) and 4′,6-diamidino-2-phenylindole (DAPI, blue) in the liver. (G) TUNEL staining of liver tissue sections and statistical analysis of TUNEL-positive cells. DCA = deoxycholic acid; TGR5 = Takeda G protein-coupled receptor 5; NF-κB = nuclear factor-kappaB; NLRP3 = NOD-like receptor family pyrin domain-containing 3; VDR = vitamin D receptor; FXR = Farnesoid X receptor; CAR = constitutive androstane receptor; PXR = pregnane X receptor; GR = glucocorticoid receptor; α5β1 = integrin alpha-5 beta-1; TLR4 = toll-like receptor 4; Myd88 = myeloid differentiation factor 88; p65 = nuclear factor-kappaB p65; p-p65 = phosphorylated-p65; IκB-α = NF-κB inhibitor alpha; GAPDH = glyceraldehyde 3-phosphate dehydrogenase; ASC = apoptosis-associated speck-like protein containing a CARD; Cas-1 = caspase-1; TNF-α = tumor necrosis factor-α; IL-1β = interleukin-1β; IL-6 = interleukin-6; TUNEL = terminal deoxynucleotidyl transferase dUTP nick-end labeling. Control, piglets were provided with basal water; SMS, piglets consumed metasilicate-based alkaline mineral water (basal water + 500 mg/L sodium metasilicate). Data are presented as the mean ± standard deviation (SD). Statistical analysis was performed using Student's *t*-tests to compare differences between the two groups. *P*-value less than 0.05 indicates a significant difference.

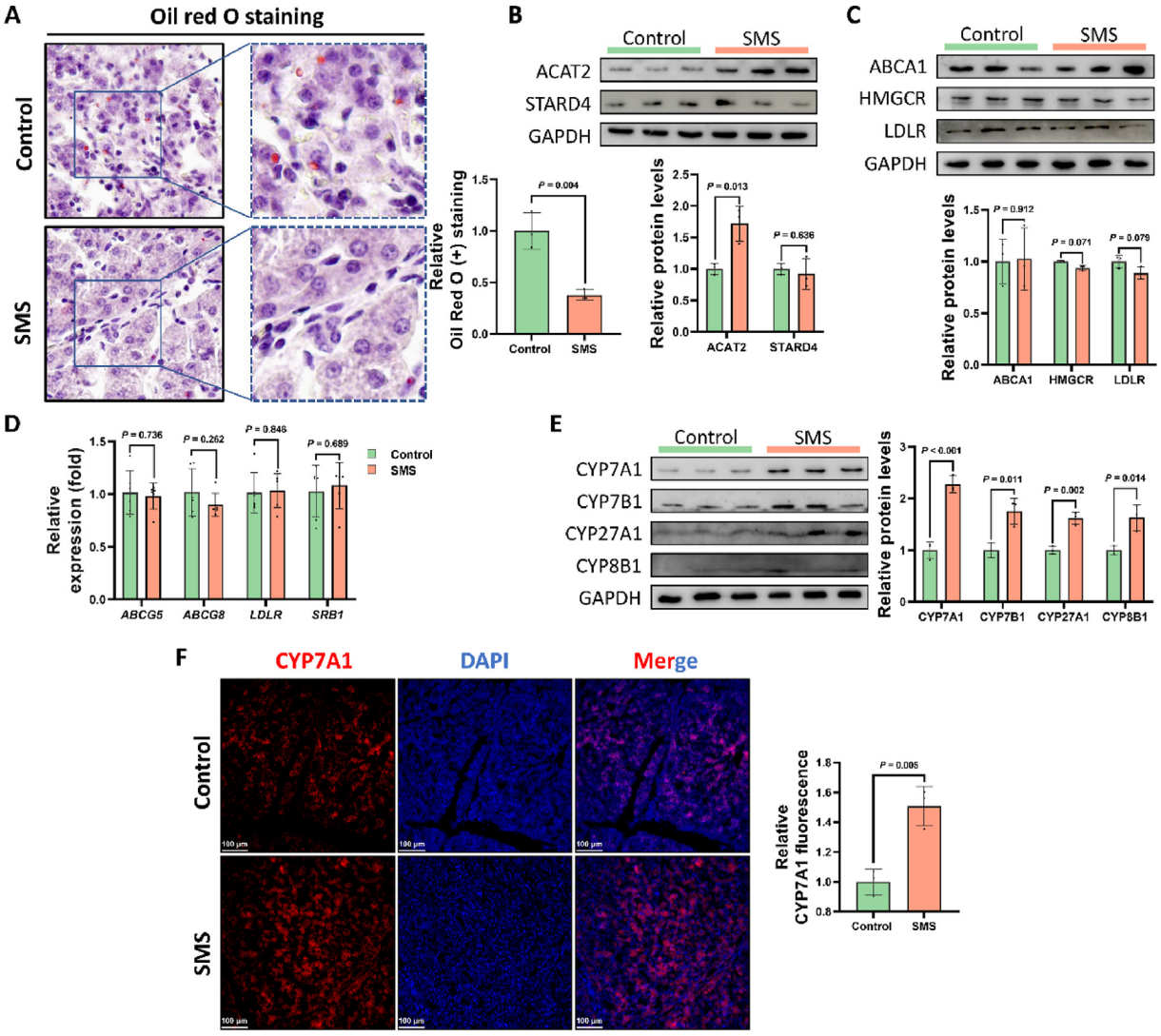

Fig. 6. Metasilicate-based alkaline mineral water maintained liver cholesterol homeostasis by regulating bile acids metabolism pathway. (A) Photomicrographs of Oil Red O staining of liver sections and statistical analysis of Oil Red O-positive staining. (B) Statistical analysis of cholesterol esterification-related proteins levels of ACAT2 and STARD4 in the liver. (C-D) Statistical analysis of cholesterol excretion/intake/biosynthesis-related (C) proteins or (D) genes expression levels in the liver. (E) Statistical analysis of cholesterol metabolism-related proteins levels of CYP7A1, CYP7B1, CYP27A1 and CYP8B1 in the liver. (F) Immunofluorescence images of CYP7A1 staining (red) and 4′,6-diamidino-2-phenylindole (DAPI, blue) in the liver and statistical analysis of CYP7A1 fluorescence intensity. ACAT2 = acyl-coenzyme A:cholesterol acyltransferase 2; STARD4 = StAR-related lipid transfer protein 4; GAPDH = glyceraldehyde 3-phosphate dehydrogenase; ABCA1 = ATP-binding cassette transporter family 361 A protein 1; HMGCR = 3-hydroxy-3-methylglutaryl-CoA reductase; LDLR = low-density lipoprotein receptor; ABCG5/8 = ATP-binding cassette subfamily G member 5/8; SRB1 = scavenger receptor class B type 1; CYP7A1 = cytochrome P450 7A1; CYP7B1 = cytochrome P450 7B1; CYP27A1 = cytochrome P450 27A1; CYP8B1 = cytochrome P450 8B1. Control, piglets were provided with basal water; SMS, piglets consumed metasilicate-based alkaline mineral water (basal water + 500 mg/L sodium metasilicate). Data are presented as the mean ± standard deviation (SD). Statistical analysis was performed using Student's *t*-tests to compare differences between the two groups. *P*-value less than 0.05 indicates a significant difference.

receptor [LDLR], $P > 0.05$ and scavenger receptor class B type 1 [*SRB1*], $P = 0.689$) in the liver of weaned piglets (Fig. 6C–D). These results reveal that SMS may facilitate the conversion of cholesterol into BA, which contributes to maintaining cholesterol homeostasis and reducing FC accumulation in the liver. As expected, classical or alternative pathways for the conversion of cholesterol to BA mediated by cytochrome P450 (CYP) enzymes were activated in the liver by SMS treatment (Fig. 6E–F), as reflected by elevated levels of CYP7A1 ($P < 0.001$ and $P = 0.005$), CYP7B1 ($P = 0.011$), CYP27A1 ($P = 0.002$) and CYP8B1 ($P = 0.014$). These results indicate that the alleviation of colonic and hepatic inflammatory responses by metasilicate-based AMW may contribute to the improvement of hepatic cholesterol and lipid metabolism disorders.

3.7. Metasilicate-based AMW maintains liver function homeostasis via L. Delbrueckii-mediated DCA-TGR5 pathway in piglets under weaning stress

To investigate whether the enrichment of *L. delbrueckii* induced by SMS could alleviate liver inflammation and cholesterol accumulation through the DCA-TGR5 pathway, we conducted a series of analyses. First, Pearson's correlation analysis revealed significant negative correlations between *L. delbrueckii* or DCA and AST and ALT levels, hepatocyte apoptosis rate, as well as cholesterol and lipid accumulation (Fig. 7A, $P < 0.05$). This further suggests that metasilicate-based AMW improves liver function via the *L. delbrueckii*-derived DCA pathway in piglets under weaning stress.

Table 4
Effect of metasilicate-based alkaline mineral water on the cholesterol levels in weaned piglets.[1]

Item	Control	SMS	SD	*P*-value
Serum, μmol/dL				
TC	36.39	27.57	3.668	0.044
FC	28.00	15.57	3.209	0.009
CEs	8.39	12.66	1.721	0.045
Liver, μmol/g				
TC	4.29	3.10	0.367	0.017
FC	3.73	1.93	0.493	0.012
CEs	0.56	1.16	0.203	0.023

TC = total cholesterol; FC = free cholesterol; CEs = cholesterol esters.
[1] Control, piglets were provided with basal water; SMS, piglets consumed metasilicate-based alkaline mineral water (basal water + 500 mg/L sodium metasilicate). Statistical significance was determined using Student's *t*-tests to compare differences between two groups; data are presented as the mean and standard deviation (SD). *P*-value less than 0.05 indicates a significant difference.

Table 5
Effect of metasilicate-based alkaline mineral water on the growth performance in weaned piglets.[1]

Item	Control	SMS	SD	*P*-value
Initial BW, kg	9.22	9.10	0.786	0.604
Final BW, kg	12.29	12.84	0.889	0.034
ADG, kg/d	0.20	0.25	0.044	<0.001
ADFI, g/d	335.7	371.9	194.70	0.615
F:G ratio	1.70	1.54	0.304	0.084

BW = body weight; ADG = average daily gain; ADFI = average daily feed intake; F:G = feed to gain ratio.
[1] Control, piglets were provided with basal water; SMS, piglets consumed metasilicate-based alkaline mineral water (basal water + 500 mg/L sodium metasilicate). Statistical significance was determined using Student's *t*-tests to compare differences between two groups; Data are presented as the mean and standard deviation (SD); *P*-value less than 0.05 indicates a significant difference.

Further analysis revealed that microbiota-mediated DCA was positively correlated with hepatic TGR5 (Fig. 7B, $P = 0.004$) and negatively correlated with inflammatory signaling markers, such as p65 (Fig. 7C, $P = 0.004$) and NLRP3 (Fig. 7D, $P = 0.004$). Furthermore, the alleviation of liver inflammation was strongly associated with the factors related to cholesterol homeostasis (Fig. 7E, $P < 0.01$). These results suggest that metasilicate-based AMW improves lipid and cholesterol homeostasis by reducing liver inflammation through the *L. delbrueckii*-DCA-TGR5 pathway.

3.8. Metasilicate-based AMW increases growth performance in piglets under weaning stress

As shown in Table 5, compared to the Control group, metasilicate-based AMW significantly increased the final BW ($P = 0.034$) and ADG ($P < 0.001$) in weaned piglets, whereas it did not affect ADFI ($P = 0.615$). In the field of economic benefits, SMS treatment reduced the F:G ($P = 0.084$) ratio in weaned piglets.

4. Discussion

The gut-liver axis refers to the mutual interaction between the gut (including its microbiota) and the liver, regulated by a comprehensive signal derived from dietary, genetic and environmental factors (Tilg et al., 2022). It plays a crucial role in nutrition, metabolism, growth, detoxification, and other physiological processes (Xu et al., 2022; Zhang et al., 2022b). This interaction is mediated by the portal vein, which allows direct transport of gut or microflora-derived products to the liver and feeds back bile or metabolite release to the gut. Recent research has uncovered that psychological or social stress, especially in early life, can cause liver injury and dysfunction and accelerate the development of liver metabolic diseases (such as MAFLD) by disturbing the gut-liver axis

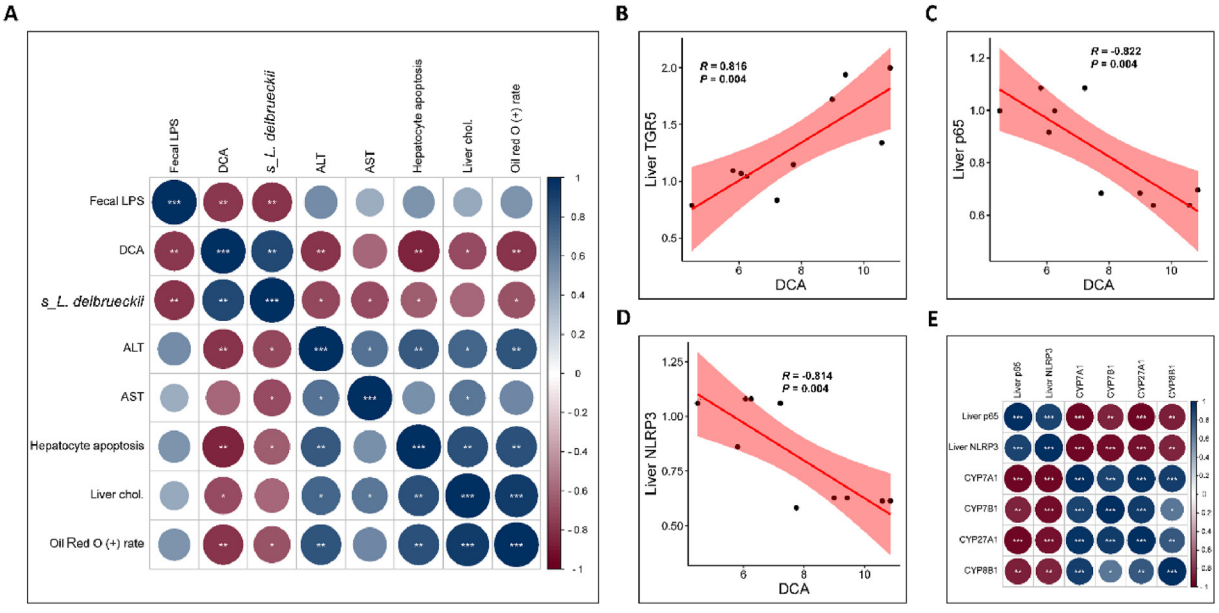

Fig. 7. Metasilicate-based alkaline mineral water maintained liver function homeostasis via *L. delbrueckii*-mediated DCA-TGR5 pathway in piglets under weaning stress. (A) Correlation analysis between the liver function-related phenotype indicators and *L. delbrueckii* or DCA. (B) Pearson correlation coefficient scatterplot between the liver TGR5 protein levels and DCA levels. (C) Pearson correlation coefficient scatterplot between the liver p65 protein levels and DCA levels. (D) Pearson correlation coefficient scatterplot between the liver NLRP3 protein levels and DCA levels. (E) Correlation analysis between the inflammatory signaling pathways activity and cholesterol metabolic enzymes. Control, piglets were provided with basal water; SMS, piglets consumed metasilicate-based alkaline mineral water (basal water + 500 mg/L sodium metasilicate). LPS = lipopolysaccharide; ALT = alanine aminotransferase; AST = aspartate aminotransferase; chol. = cholesterol; *L. delbrueckii* = *Lactobacillus_delbrueckii*; DCA = deoxycholic acid; TGR5 = Takeda G protein-coupled receptor 5; p65 = nuclear factor-kappaB p65; NLRP3 = NOD-like receptor family pyrin domain-containing 3; CYP7A1 = cytochrome P450 7A1; CYP7B1 = cytochrome P450 7B1; CYP27A1 = cytochrome P450 27A1; CYP8B1 = cytochrome P450 8B1. *P*-value less than 0.05 indicates a significant difference. *$P < 0.05$, **$P < 0.01$, and ***$P < 0.001$.

homeostasis (Demori and Grasselli, 2023; Ringseis and Eder, 2022; Xu et al., 2022). For piglets, it is difficult to avoid being exposed to a variety of stressors. Hence, developing targeted drugs or strategies to maintain gut-liver axis homeostasis is of great significance for piglets at risk of stress exposure (Chen et al., 2024b). In the present study, we found that metasilicate-based AMW maintains gut-liver axis homeostasis by ameliorating colonic and hepatic inflammatory responses and hepatic cholesterol metabolism through the microbiota-mediated SBA pathway in piglets under weaning stress. Importantly, metasilicate-based AMW-mediated gut-liver axis homeostasis enhancement significantly improved growth performance in weaned piglets.

Research from the last few years has convincingly proven that an impaired gut barrier is a prerequisite for a disturbed gut-liver axis (Zhang et al., 2022b). Maintaining the integrity of the intestinal epithelial barrier is crucial as it acts as a vital defense line, protecting the liver from antigens, metabolites, and potential intestinal microbes (Tilg et al., 2022). Various studies demonstrated that weaning or other early-life stress can evoke colonic epithelial damage and dysbiosis in piglets, which in turn affect nutrient absorption and growth (Campbell et al., 2013; Gresse et al., 2021; Vogel et al., 2020). This is consistent with the present study, where we found that early weaning stress-induced severe colonic epithelial damage and loss of epithelial cells. Importantly, H&E staining results showed that metasilicate-based AMW therapy effectively mitigated the loss of gut barrier integrity caused by weaning stress, which is critical for piglets with immature immune systems. The gut barrier operates through various mechanisms, including microbiota—host interactions and regulation of intestinal inflammation (Zhang et al., 2024b; Hu et al., 2024). Therefore, the observed reduction in epithelial injury in weaned piglets may be linked to changes in microflora composition induced by metasilicate-based AMW.

The colon, due to its anaerobic environment and low fecal fluidity, provides an ideal cavity for microbiota richness and colonization (Moran and Jackson, 1992). The microbiota community is pivotal in maintaining gut-liver axis homeostasis and is a part of this bidirectional interaction (Zhang et al., 2022b). Consequently, improving microflora composition via dietary or therapeutic interventions may be an effective strategy for treating diseases involving gut-liver axis disorders. Growing evidence indicates that weaning stress in piglets leads to colonic microbiota dysbiosis, characterized by the enrichment of harmful bacteria and suppression of beneficial bacteria (Liu et al., 2019; Tian et al., 2022). Our results confirm that metasilicate-based AMW serves as a microbiota modulator that significantly changes the microbiota structure in the colonic contents of weaned piglets. Specifically, SMS treatment promoted the abundance of Firmicutes in colonic feces, as reflected by an increased abundance of *Lactobacillus*. It is well known that *Lactobacillus* is recognized widely as a probiotic, exhibits anti-inflammatory properties, strengthens the gut barrier, and modulates immunity (Rastogi and Singh, 2022). Furthermore, *Lactobacillus* can competitively inhibit opportunistic pathogens from adhering to the epithelium, thus protecting against colonization by harmful microbes (Rastogi and Singh, 2022; Xiao et al., 2020). This mechanism may explain the observed reduction in the *Prevotella* genus in colon content after metasilicate-based AMW treatment. *Prevotella*, a gram-negative bacteria producer of LPS, is associated with chronic inflammation (Larsen, 2017). These findings underscore that metasilicate-based AMW preserves the positive effects of gut-liver axis mediators, the gut microflora, by elevating beneficial bacteria and inhibiting detrimental bacteria colonization in weaned piglets.

LEfSe analysis is a recognized method for identifying marker microflora in the host between different treatment groups (Chen et al., 2023a). In this study, we observed a shift in the dominant microbiota in the colon after SMS treatment. It is worth highlighting that the dominant bacterium in piglets drinking metasilicate-based AMW was *L. delbrueckii*, a member of the *Lactobacillus* genus. *L. delbrueckii* has demonstrated potential psychobiological activity, alleviating anxiety-like behavior in zebrafish, which suggests its antistress potential (Olorocisimo et al., 2023). Additionally, a previous study has shown that *L. delbrueckii* improves gut barrier integrity and antioxidant capacity in weaned piglets exposed to LPS (Chen et al., 2020). This aligns with our observations, suggesting that the alleviation of colonic epithelial damage by SMS treatment is linked to improved dominant microflora.

The symbiotic microbiota, known as microbial organs, have coevolved with their hosts over long periods, mediating various physiological and metabolic processes (Rastogi and Singh, 2022). Given the shift in dominant bacteria between the two groups, we speculated that the interaction patterns among microflora communities were altered, subsequently affecting the functional profile of the microflora. Our results confirmed this speculation: *Lactobacillus*, as the dominant genus in piglets in the SMS treatment group, played a more positive role within the microbiota communities and significantly improved their functional profile. Of note, SMS treatment reduced the gene abundance related to apoptosis and disease infection. Moreover, it significantly decreased the gene abundance associated with MAFLD while promoting the gene enrichment of SBA synthesis in the colonic microflora of weaned piglets. These enriched genes form a complete signaling chain related to the regulation of the gut-liver axis. We speculated that SMS treatment improved microbiota composition and promoted microbiota-mediated SBA biosynthesis to maintain gut-liver axis homeostasis through the SBA receptor pathway in piglets under weaning stress.

The colonic marker community in SMS-treated piglets, *Lactobacillus*, has been reported to regulate cholesterol metabolism and gut-derived metabolite production, such as short-chain fatty acids (SCFA), LPS, and BA (Hou et al., 2020; Mantegazza et al., 2018). As expected, LPS levels in colonic feces were decreased after SMS treatment, which may be a consequence of the elevated *Lactobacillus* genus and the reduced *Prevotella* genus. On the other hand, SBA generated by certain communities is involved in maintaining liver homeostasis by targeting their cellular receptors (Chen et al., 2019). BA is converted from cholesterol in the liver and released into the gut through the bile duct; Once in the colon, enteric bacteria deconjugate the primary BA into its secondary forms, mainly DCA and LCA (Chen et al., 2019; Zhang et al., 2022a). In this study, there was no difference in serum TBA levels between the two groups. Notably, SMS treatment promoted microbiota-mediated DCA biosynthesis. Currently, SBA biosynthesis is reported to be associated with specific bacterial genera such as *Lactobacillus*, *Bacteroidetes*, and *Eubacteria*, with ongoing research likely to expand this list (Funabashi et al., 2020). Our results showed that the DCA levels in colonic feces were highly positively correlated with *L. delbrueckii* abundance, suggesting a pivotal role for the *L. delbrueckii*-mediated DCA biosynthesis pathway in SMS-induced gut-liver axis homeostasis. Convincing evidence exists in the literature that SBA, such as DCA, inhibits NF-κB signaling by activating SBA receptors, including CAR, PXR, and TGR5, to alleviate inflammatory response (Hu et al., 2021; Zhao et al., 2023). The results of this study indicated that SMS-mediated microbiota-derived DCA restricted pro-inflammatory cytokine release and alleviated weaning stress-induced colonic inflammation. This is related to the activation of SBA receptors TGR, CAR and PXR, which in turn inhibits the NF-κB pathway. Evidence suggests that colonic SBA, such as DCA, activate PXR in epithelial cells, enhancing *TGF-β* expression while suppressing TLR4-dependent pro-inflammatory cytokine

production (Chen et al., 2019). Similar effects were observed for other BA receptors, including CAR and TGR5. Therefore, the increased levels of colonic TGF-β levels and reduced macrophage infiltration further underscored the anti-inflammatory effects of metasilicate-based AMW.

Our results demonstrated that metasilicate-based AMW maintains gut homeostasis in weaned piglets by improving microbiota composition and microbiota-derived SBA. However, whether DCA improves liver function through a similar mechanism remains unclear. It is well known that various liver diseases are characterized by an impaired gut barrier and a disturbed gut-liver axis (Tilg et al., 2022). Epithelial barrier damage promotes the entry of bacterial components like LPS into the portal vein, causing liver inflammation and lipid metabolism disorders (Ringseis and Eder, 2022). In this study, SMS treatment reduced the gut barrier permeability in weaned piglets, as evidenced by decreased serum levels of DAO and LPS. Additionally, improvements in liver function and reduced liver injury were observed in piglets under weaning stress after SMS treatment. We speculated that the improvement in liver function was related to microbiota-derived DCA and the activation of the SBA receptor pathway. By analyzing the expression of SBA receptors, we found that only *TGR5* expression was activated by SMS treatment in the liver. A previous study confirmed that DCA-mediated TGR5 activation inhibits the NF-κB/NLRP3 pathways in mastitis caused by *Staphylococcus aureus* (Guo et al., 2016), which is consistent with our study. Metasilicate-based AMW inhibited the canonical inflammatory signaling pathways NF-κB and NLRP3, reduced pro-inflammatory cytokine expression, and alleviated hepatic macrophage infiltration. Interestingly, the reduction of the inflammatory response induced by SMS further rescued hepatocyte apoptosis. These results highlight potential strategies to intervene in gut-liver axis homeostasis by modulating gut microbial metabolism.

On the other hand, there is a high correlation between weaning-induced psychological or social stress and MAFLD, which may be linked to disturbed hepatic cholesterol metabolism. Numerous studies have found that stress-induced increases in cortisol or corticosterone led to liver cholesterol accumulation and disordered lipid metabolism in both humans and experimental animals (Fraser et al., 1999; Solomon et al., 2011). In this study, metasilicate-based AMW notably attenuated lipids and cholesterol accumulation induced by weaning stress and promoted the conversion of toxic molecule FC into CEs by activating *ACAT2* expression, thus reducing liver lipotoxicity in weaned piglets. Of note, metasilicate-based AMW did not affect the expression of proteins related to cholesterol excretion, intake, or biosynthesis pathways. To our knowledge, there are no reports on the regulation of cholesterol metabolism by metasilicate AMW and its related mechanisms. However, the hypocholesterolemic effect of *Lactobacillus* has been extensively reported in animal and clinical studies, primarily involving the regulation of key enzymes that convert cholesterol into BA (Guo et al., 2018; Wang et al., 2019). The conversion of cholesterol to BA occurs via two main pathways: the neutral (classic) pathway, mediated by CYP7A1 and CYP8B1 in the liver, and a fraction of the BA "pool" synthesized via the acidic (alternative) pathway, which is initiated by CYP27A1 and CYP7B1 (Wei et al., 2023; Zhao et al., 2023). Our results indicate that metasilicate-based AMW maintains its metabolic homeostasis by promoting cholesterol conversion and the expression of these BA synthases. Importantly, correlation analysis showed that *L. delbrueckii* and its-mediated DCA were negatively correlated with liver function markers (ALT and AST) and lipid and cholesterol accumulation, further indicating that SMS-induced improvement of microflora composition maintains the functional homeostasis of the gut-liver axis through the SBA pathway. Evidence suggests that weaning stress-induced gut barrier disruption promotes the entry of LPS and pro-inflammatory factors into the portal vein, aggravating preexisting liver disease through hepatic inflammation (Ringseis and Eder, 2022; Tilg et al., 2022). Therefore, relief of liver inflammation may contribute to cholesterol homeostasis (Zhao et al., 2023). This coincided with our findings that microflora-mediated DCA was positively correlated with liver TGR5 while being negatively correlated with key proteins of the inflammatory pathway (NF-κB and NLRP3). Moreover, these two key factors, NF-κB and NLRP3, were negatively correlated with cholesterol metabolism enzymes, including CYP7A1, CYP7B1, CYP27A1, and CYP8B1. These results suggest that metasilicate-based AMW improves liver functional homeostasis through the DCA/TGR5-mediated gut-liver axis in piglets under weaning stress.

5. Conclusion

In conclusion, our study demonstrates, for the first time, that metasilicate-based AMW improves the growth performance of weaned piglets by maintaining gut-liver axis homeostasis through the microbiota-mediated SBA pathway. Further analysis showed that the *L. delbrueckii*-derived DCA is a key mediator in this process. Mechanically, metasilicate-based AMW promotes DCA biosynthesis by elevating the abundance of *L. delbrueckii* in the colon and then improves weaning-induced colonic and liver injury, the inflammatory response, and liver cholesterol homeostasis by targeting the DCA-SBA receptors—NF—κB/NLRP3 pathways. Our findings may provide a new strategy for metasilicate-based AMW in the prevention and treatment of stress-induced gut-liver axis dysfunction in mammals.

Credit Author Statement

Jian Chen: Writing — review & editing, Writing — original draft, Visualization, Software, Resources, Methodology, Investigation, Formal analysis, Data curation, Conceptualization. **Kanwar K. Malhi:** Writing — review & editing, Visualization, Resources, Investigation, Formal analysis, Conceptualization. **Xiaowei Li:** Visualization, Validation, Software, Resources, Methodology, Formal analysis, Data curation. **Xiangwen Xu:** Software, Resources, Methodology, Investigation, Data curation, Conceptualization. **Jianxun Kang:** Validation, Software, Resources, Investigation, Formal analysis, Data curation, Conceptualization. **Bichen Zhao:** Validation, Software, Resources, Methodology, Formal analysis, Data curation. **Yaru Xu:** Visualization, Validation, Software, Resources, Formal analysis, Data curation. **Xuenan Li:** Validation, Supervision, Software, Resources, Methodology, Investigation, Funding acquisition, Data curation. **Jinlong Li:** Writing — review & editing, Visualization, Supervision, Investigation, Funding acquisition, Conceptualization.

Declaration of competing interest

We declare that we have no financial and personal relationships with other people or organizations that can inappropriately influence our work, and there is no professional or other personal interest of any nature or kind in any product, service and/or company that could be construed as influencing the content of this paper.

Acknowledgements

This study has received assistance from National Natural Science Foundation of China (No. 32402972 and No. W2433075), Postdoctoral Fellowship Program of CPSF (No. GZB20240133) and China Agriculture Research System of MOF and MARA (No. CARS-35). The

authors thank the Jinlong Li Laboratory of College of Veterinary Medicine at the Northeast Agricultural University for technical support. We acknowledge Qinglin Li, Dr. Song Qi, and all members of Nail Biotechnology Co. Ltd. (Beijing, China) for their assistance in this study.

Appendix A. Supplementary data

Supplementary data to this article can be found online at https://doi.org/10.1016/j.aninu.2024.09.003.

References

Bellia JP, Birchall JD, Roberts NB. Beer: a dietary source of silicon. Lancet 1994;343:235.
Campbell JM, Crenshaw JD, Polo J. The biological stress of early weaned piglets. J Anim Sci Biotechnol 2013;4:19.
Carpino G, Overi D, Onori P, Franchitto A, Cardinale V, Alvaro D, et al. Effect of calcium-sulphate-bicarbonate water in a murine model of non-alcoholic fatty liver disease: a histopathology study. Int J Mol Sci 2022;23:10065.
Chen F, Wang H, Chen J, Liu Y, Wen W, Li Y, et al. Lactobacillus delbrueckii ameliorates intestinal integrity and antioxidant ability in weaned piglets after a lipopolysaccharide challenge. Oxid Med Cell Longev 2020;2020:6028606.
Chen J, Xu YR, Kang JX, Zhao BC, Dai XY, Qiu BH, Li JL. Effects of alkaline mineral complex water supplementation on growth performance, inflammatory response, and intestinal barrier function in weaned piglets. J Anim Sci 2022;100(10):skac251.
Chen J, Dai XY, Li XW, Tang YX, Xu XW, Li JL. Lycopene mitigates atrazine-induced hypothalamic neural stem cell senescence by modulating the integrated stress response pathway. Phytomedicine 2024a;135:156114.
Chen J, Dai XY, Zhao BC, Xu XW, Kang JX, Xu YR, et al. Role of the GLP2-Wnt1 axis in silicon-rich alkaline mineral water maintaining intestinal epithelium regeneration in piglets under early-life stress. Cell Mol Life Sci 2024b;81(1):126.
Chen J, Xu XW, Kang JX, Zhao BC, Xu YR, Li JL. Metasilicate-based alkaline mineral water confers diarrhea resistance in maternally separated piglets via the microbiota-gut interaction. Pharmacol Res 2023a;187:106580.
Chen J, Zhao BC, Dai XY, Xu YR, Kang JX, Li JL. Drinking alkaline mineral water confers diarrhea resistance in maternally separated piglets by maintaining intestinal epithelial regeneration via the brain-microbe-gut axis. J Adv Res 2023b;52:29–43.
Chen ML, Takeda K, Sundrud MS. Emerging roles of bile acids in mucosal immunity and inflammation. Mucosal Immunol 2019;12:851–61.
Dai XY, Li XW, Zhu SY, Li MZ, Zhao Y, Talukder M, et al. Lycopene ameliorates di(2-ethylhexyl) phthalate-induced pyroptosis in spleen via suppression of classic caspase-1/NLRP3 pathway. J Agric Food Chem 2021;69:1291–9.
Dai XY, Zhu SY, Chen J, Li MZ, Talukder M, Li JL. Role of toll-like receptor/MyD88 signaling in lycopene alleviated di-2-ethylhexyl phthalate (DEHP)-Induced inflammatory response. J Agric Food Chem 2022;70:10022–30.
Demori I, Grasselli E. The role of the stress response in metabolic dysfunction-associated fatty liver disease: a psychoneuroendocrineimmunology-based perspective. Nutrients 2023;15:795.
Ding A, Wen X. Dandelion root extract protects NCM460 colonic cells and relieves experimental mouse colitis. J Nat Med 2018;72:857–66.
Eslam M, Newsome PN, Sarin SK, Anstee QM, Targher G, Romero-Gomez M, et al. A new definition for metabolic dysfunction-associated fatty liver disease: an international expert consensus statement. J Hepatol 2020;73:202–9.
Fraser R, Ingram MC, Anderson NH, Morrison C, Davies E, Connell JM. Cortisol effects on body mass, blood pressure, and cholesterol in the general population. Hypertension 1999;33:1364–8.
Funabashi M, Grove TL, Wang M, Varma Y, McFadden ME, Brown LC, et al. A metabolic pathway for bile acid dehydroxylation by the gut microbiome. Nature 2020;582:566–70.
Galluzzi L, Yamazaki T, Kroemer G. Linking cellular stress responses to systemic homeostasis. Nat Rev Mol Cell Biol 2018;19:731–45.
Gimsa U, Bruckmann R, Tuchscherer A, Tuchscherer M, Kanitz E. Early-life maternal deprivation affects the mother-offspring relationship in domestic pigs, as well as the neuroendocrine development and coping behavior of piglets. Front Behav Neurosci 2022;16:980350.
Gresse R, Chaucheyras-Durand F, Denis S, Beaumont M, Van de Wiele T, Forano E, et al. Weaning-associated feed deprivation stress causes microbiota disruptions in a novel mucin-containing *in vitro* model of the piglet colon (MPigut-IVM). J Anim Sci Biotechnol 2021;12:75.
Gunathilaka BE, Medagoda N, Cha JH, Yoo BW, Choi SI, Shin CH, et al. Effects of a dietary anionic alkali mineral complex in juvenile olive flounder (Paralichthys olivaceus) during low water temperature season. Aquacult Rep 2022;27:101420.
Guo C, Xie S, Chi Z, Zhang J, Liu Y, Zhang L, et al. Bile acids control inflammation and metabolic disorder through inhibition of NLRP3 inflammasome. Immunity 2016;45:802–16.
Guo CF, Zhang S, Yuan YH, Li JY, Yue TL. Bile salt hydrolase and S-layer protein are the key factors affecting the hypocholesterolemic activity of Lactobacillus casei-fermented milk in hamsters. Mol Nutr Food Res 2018;62:e1800728.
Hu ZY, Yang SJ, Chang YH, Wang XQ, Liu RQ, Jiang FW, et al. AHR activation relieves deoxynivalenol-induced disruption of porcine intestinal epithelial barrier functions. J Hazard Mater 2024;480:136095.
Hou G, Peng W, Wei L, Li R, Yuan Y, Huang X, et al. Lactobacillus delbrueckii interfere with bile acid enterohepatic circulation to regulate cholesterol metabolism of growing-finishing pigs via its bile salt hydrolase activity. Front Nutr 2020;7:617676.
Hu J, Wang C, Huang X, Yi S, Pan S, Zhang Y, et al. Gut microbiota-mediated secondary bile acids regulate dendritic cells to attenuate autoimmune uveitis through TGR5 signaling. Cell Rep 2021;36:109726.
Jugdaohsingh R, Calomme MR, Robinson K, Nielsen F, Anderson SH, D'Haese P, et al. Increased longitudinal growth in rats on a silicon-depleted diet. Bone 2008;43:596–606.
Jurkic LM, Cepanec I, Pavelic SK, Pavelic K. Biological and therapeutic effects of ortho-silicic acid and some ortho-silicic acid-releasing compounds: new perspectives for therapy. Nutr Metab 2013;10:2.
Kim EJ, Bu SY, Sung MK, Kang MH, Choi MK. Analysis of antioxidant and anti-inflammatory activity of silicon in murine macrophages. Biol Trace Elem Res 2013;156:329–37.
Larsen JM. The immune response to Prevotella bacteria in chronic inflammatory disease. Immunology 2017;151:363–74.
Lei Y, Tang L, Chen Q, Wu L, He W, Tu D, et al. Disulfiram ameliorates nonalcoholic steatohepatitis by modulating the gut microbiota and bile acid metabolism. Nat Commun 2022;13:6862.
Li XW, Li S, Yang Y, Talukder M, Xu XW, Li CX, et al. The FAK/occludin/ZO-1 complex is critical for cadmium-induced testicular damage by disruption of the integrity of the blood-testis barrier in chickens. J Hazard Mater 2024;470:134126.
Liu G, Zheng J, Wu X, Xu X, Jia G, Zhao H, et al. Putrescine enhances intestinal immune function and regulates intestinal bacteria in weaning piglets. Food Funct 2019;10:4134–42.
Mantegazza C, Molinari P, D'Auria E, Sonnino M, Morelli L, Zuccotti GV. Probiotics and antibiotic-associated diarrhea in children: a review and new evidence on Lactobacillus rhamnosus GG during and after antibiotic treatment. Pharmacol Res 2018;128:63–72.
Monte F, Cebe T, Ripperger D, Ighani F, Kojouharov HV, Chen BM, et al. Ionic silicon improves endothelial cells' survival under toxic oxidative stress by overexpressing angiogenic markers and antioxidant enzymes. J Tissue Eng Regen Med 2018;12:2203–20.
Moran BJ, Jackson AA. Function of the human colon. Br J Surg 1992;79:1132–7.
NRC. NRC (national research council). Nutrient requirements of swine. 10th ed. Washington, DC: The National Academy Press; 2012. 2012.
O'Mahony SM, Marchesi JR, Scully P, Codling C, Ceolho AM, Quigley EM, et al. Early life stress alters behavior, immunity, and microbiota in rats: implications for irritable bowel syndrome and psychiatric illnesses. Biol Psychiatr 2009;65:263–7.
Olorocisimo JP, Diaz LA, Co DE, Carag HM, Ibana JA, Velarde MC. Lactobacillus delbrueckii reduces anxiety-like behavior in zebrafish through a gut microbiome - brain crosstalk. Neuropharmacology 2023;225:109401.
Pabst O, Hornef MW, Schaap FG, Cerovic V, Clavel T, Bruns T. Gut-liver axis: barriers and functional circuits. Nat Rev Gastroenterol Hepatol 2023;20:447–61.
Rastogi S, Singh A. Gut microbiome and human health: exploring how the probiotic genus Lactobacillus modulate immune responses. Front Pharmacol 2022;13:1042189.
Ringseis R, Eder K. Heat stress in pigs and broilers: role of gut dysbiosis in the impairment of the gut-liver axis and restoration of these effects by probiotics, prebiotics and synbiotics. J Anim Sci Biotechnol 2022;13:126.
Shi YS, Yang TN, Wang YX, Ma XY, Liu S, Zhao Y, et al. Melatonin Mitigates Atrazine-Induced Renal Tubular Epithelial Cell Senescence by Promoting Parkin-Mediated Mitophagy. Research 2024;7:0378.
Solomon MB, Sakai RR, Woods SC, Foster MT. Differential effects of glucocorticoids on energy homeostasis in Syrian hamsters. Am J Physiol Endocrinol Metab 2011;301:E307–16.
Tian S, Wang J, Wang J, Zhu W. Differential effects of early-life and post-weaning galacto-oligosaccharide intervention on colonic bacterial composition and function in weaning piglets. Appl Environ Microbiol 2022;88:e0131821.
Tilg H, Adolph TE, Trauner M. Gut-liver axis: pathophysiological concepts and clinical implications. Cell Metabol 2022;34:1700–18.
Vogel SC, Brito NH, Callaghan BL. Early life stress and the development of the infant gut microbiota: implications for mental health and neurocognitive development. Curr Psychiatr Rep 2020;22:61.
Wang G, Huang W, Xia Y, Xiong Z, Ai L. Cholesterol-lowering potentials of Lactobacillus strain overexpression of bile salt hydrolase on high cholesterol diet-induced hypercholesterolemic mice. Food Funct 2019;10:1684–95.
Wei X, Yin F, Wu M, Xie Q, Zhao X, Zhu C, et al. G protein-coupled receptor 35 attenuates nonalcoholic steatohepatitis by reprogramming cholesterol homeostasis in hepatocytes. Acta Pharm Sin B 2023;13:1128–44.
Woods CP, Hazlehurst JM, Tomlinson JW. Glucocorticoids and non-alcoholic fatty liver disease. J Steroid Biochem Mol Biol 2015;154:94–103.
Xiao Y, Zhao J, Zhang H, Zhai Q, Chen W. Mining Lactobacillus and Bifidobacterium for organisms with long-term gut colonization potential. Clin Nutr 2020;39:1315–23.

Xu MY, Guo CC, Li MY, Lou YH, Chen ZR, Liu BW, et al. Brain-gut-liver axis: chronic psychological stress promotes liver injury and fibrosis via gut in rats. Front Cell Infect Microbiol 2022;12:1040749.
Zhang C, Liu Y, Wang P, Wang B, Zhang S, Hua Z, et al. Effects of Se-enriched yeast on the amelioration of atrazine-induced meat quality degradation. Food Chem 2024a;454:139737.
Zhang P, Zheng L, Duan Y, Gao Y, Gao H, Mao D, et al. Gut microbiota exaggerates triclosan-induced liver injury via gut-liver axis. J Hazard Mater 2022a;421:126707.
Zhang S, Song W, Hua Z, Du J, Lucena RB, Wang X, et al. Overview of T-2 Toxin Enterotoxicity: From Toxic Mechanisms and Detoxification to Future Perspectives. J Agric Food Chem 2024b;72(7):3314–24.
Zhang X, Liu H, Hashimoto K, Yuan S, Zhang J. The gut-liver axis in sepsis: interaction mechanisms and therapeutic potential. Crit Care 2022b;26:213.
Zhao C, Wu K, Hao H, Zhao Y, Bao L, Qiu M, et al. Gut microbiota-mediated secondary bile acid alleviates Staphylococcus aureus-induced mastitis through the TGR5-cAMP-PKA-NF-kappaB/NLRP3 pathways in mice. NPJ Biofilm Microbiom 2023;9:8.
Zhao Y, Chang YH, Ren HR, Lou M, Jiang FW, Wang JX, et al. Phthalates induce neurotoxicity by disrupting the Mfn2-PERK axis-mediated endoplasmic reticulum-mitochondria interaction. J Agric Food Chem 2024;72:7411–22.
Zhao Y, Li XN, Zhang H, Cui JG, Wang JX, Chen MS, et al. Phthalate-induced testosterone/androgen receptor pathway disorder on spermatogenesis and antagonism of lycopene. J Hazard Mater 2022;439:129689.